

An analysis of *CoRoT* multicolour photometry of exoplanets [★]

F. Borsa^{1,2†} and E. Poretti²

¹Università dell’Insubria - Dipartimento di Scienza e Alta Tecnologia, Via Valleggio 11, 22100 Como, Italy

²INAF – Osservatorio Astronomico di Brera, Via E. Bianchi 46, 23807 Merate (LC), Italy

Accepted 2012 September 26. Received 2012 September 17; in original form 2012 July 13

ABSTRACT

We analysed the chromatic data of the planetary transits observed with *CoRoT* to supply homogeneous time series in each of the *CoRoT* colours. In a first step, we cleaned the chromatic light curves from the contamination of nearby stars and removed outliers and trends caused by anything different from the planetary transits. Then, we simultaneously fitted the chromatic transits of each planet, obtaining a common solution for the orbital parameters i , t_0 and a/R_s , with a particular care in the fitting for different limb-darkening parameters. The planet-to-star radius ratios in the *CoRoT* colours are compatible when considering one planet at a time, but the ensemble of low-mass planets seems to show a peculiar behaviour of the radius ratios.

Key words: methods: data analysis – techniques: photometric – planetary systems.

1 INTRODUCTION

The discovery of new planets is recurrent news in the exploitation of ground-based surveys (e.g., Mayor et al. 2011) and space missions (e.g., Borucki et al. 2011). We count more than 700 confirmed detections and a lot of candidates are in the waiting list. Therefore, it is quite natural to direct our attention to techniques that can help in disentangling the uncertain cases and/or supply more information on the planet’s structure. If we are able to point out any kind of new feature, this can help in planning future investigations and/or theoretical analysis.

Kepler and *CoRoT* (convection, rotation and planetary transits; Baglin et al. 2006) space missions make use of the photometric method of transits to detect exoplanets. Theory predicts that the depth of the transit of a planetary body in front of its parent star should not depend on the wavelength, except for the effect of the stellar limb darkening. However this is true only at first order: the apparent radius of the planet, and therefore its transit depth, does depend on the wavelength; the light from the parent star filters through the planet’s atmosphere, so that the atmospheric signatures remain imprinted in the transit depths at different wavelengths, creating a transmission spectrum. The weight of this effect depends on the atmospheric scale height. After the first *Hubble Space Telescope* positive result in 2002, the detection of spectral features in the exoplanet atmospheres over a broad wavelength range is now a firmly established field (Seager & Deming 2010).

In the case of the *CoRoT* mission, a chromatic device was mounted in the focal block with the aim of discriminating ‘nearly achromatic planetary transits from coloured stellar fluctuations’

(Barge et al. 2006). The light passes through a prism before entering in the exoplanet channel: to obtain chromatic light curves, the mask is divided into three submasks along the dispersion direction. The mask (and so the relative submasks) for each target has a shape optimized for the magnitude and location of nearby fainter stars. Such a shape is chosen between a set of templates in order to maximize the signal-to-noise ratio (S/N). The chromatic device plays an important role in the selection of the most promising targets, allowing the rejection of several false positives (Carpano et al. 2009), and the confirmation of the planetary nature of objects like *CoRoT*-7b (Léger et al. 2009) and *CoRoT*-8b (Bordé et al. 2010).

The specificity of each mask constitutes a great difficulty in extracting physical parameters from the coloured light curves, but the efforts involved could be rewarding. Indeed, the detection of small differences in the amplitudes and in the phases of the chromatic light curves of the high-amplitude δ Sct star *CoRoT* 101155310 allowed us to discriminate between the radial and non-radial nature of the pulsation mode (Poretti et al. 2011). Therefore, we considered it noteworthy to undertake a study of the chromatic light curves of the first planets discovered by *CoRoT* to point out the useful hints that this unique photometric device can supply for further investigations.

2 DATA ANALYSIS

At the time of our analysis, *CoRoT* has discovered 23 planets, of which only the first 15 have public data. Among these 15 planets, only 10 belong to the subset for which chromatic data are available: our analysis focused on these targets (Table 1).

2.1 Removing contamination

The point spread function (PSF) of the *CoRoT* optics is highly defocused, to improve the photometric precision and to reduce the

[★] The *CoRoT* space mission was developed and is operated by the French space agency CNES, with participation of ESA’s RSSD and Science Programmes, Austria, Belgium, Brazil, Germany, and Spain.

[†] E-mail: francesco.borsa@brera.inaf.it

Table 1. Estimates of the contamination factors in each mask (white) and submask (red, green, blue) for the 10 *CoRoT* planets analysed, and characteristics of the parent stars. Nearby stars have been considered up to a 20 arcsec distance from the source.

Planet	<i>CoRoT</i> colour contamination				Parent Star	<i>V</i> mag	Contaminants Num.	<i>V</i> mag range	Discovery paper
	White (per cent)	Red (per cent)	Green (per cent)	Blue (per cent)					
CoRoT-1b	1.02 ^{+0.31} _{-0.23}	1.43 ^{+0.44} _{-0.32}	0.36 ^{+0.14} _{-0.11}	0.16 ^{+0.07} _{-0.06}	G0 V	13.62	6	17.25 - 20.50	Barge et al. (2008)
CoRoT-2b	5.09 ^{+0.60} _{-0.53}	2.94 ^{+0.58} _{-0.52}	6.41 ^{+1.27} _{-1.14}	11.95 ^{+1.72} _{-1.53}	G7 V	12.57	9	15.60 - 20.28	Alonso et al. (2008)
CoRoT-4b	0.01 ^{+0.00} _{-0.00}	0.01 ^{+0.00} _{-0.00}	0.00 ^{+0.00} _{-0.00}	0.00 ^{+0.00} _{-0.00}	F8 V	13.69	6	17.84 - 20.38	Aigrain et al. (2008)
CoRoT-5b	3.28 ^{+0.90} _{-0.61}	2.59 ^{+0.87} _{-0.65}	1.55 ^{+0.50} _{-0.33}	6.38 ^{+1.50} _{-1.18}	F9 V	14.02	6	16.19 - 20.32	Rauer et al. (2009)
CoRoT-6b	0.96 ^{+0.24} _{-0.16}	1.12 ^{+0.32} _{-0.21}	0.42 ^{+0.11} _{-0.09}	0.60 ^{+0.22} _{-0.17}	F9 V	13.91	6	16.59 - 20.58	Fridlund et al. (2010)
CoRoT-7b	0.71 ^{+0.19} _{-0.19}	0.08 ^{+0.03} _{-0.02}	0.08 ^{+0.02} _{-0.02}	3.77 ^{+1.11} _{-1.18}	K0 V	11.67	6	13.65 - 18.96	Leger et al. (2009)
CoRoT-8b	0.96 ^{+0.24} _{-0.20}	0.71 ^{+0.26} _{-0.19}	0.22 ^{+0.07} _{-0.05}	2.79 ^{+0.83} _{-0.91}	K1 V	14.30	6	18.30 - 20.10	Bordé et al. (2010)
CoRoT-9b	0.56 ^{+0.13} _{-0.13}	0.08 ^{+0.02} _{-0.01}	0.02 ^{+0.02} _{-0.01}	3.01 ^{+0.74} _{-0.70}	G3 V	13.69	6	15.04 - 20.68	Deeg et al. (2010)
CoRoT-11b	4.00 ^{+0.65} _{-0.55}	5.17 ^{+0.99} _{-0.82}	1.08 ^{+0.37} _{-0.23}	1.90 ^{+0.44} _{-0.34}	F6 V	12.94	7	16.35 - 20.60	Gandolfi et al. (2010)
CoRoT-3b	7.02 ^{+0.97} _{-0.84}	2.19 ^{+0.45} _{-0.41}	11.14 ^{+1.99} _{-1.84}	17.60 ^{+3.49} _{-2.74}	F3 V	13.29	9	14.60 - 21.13	Deleuil et al. (2008)

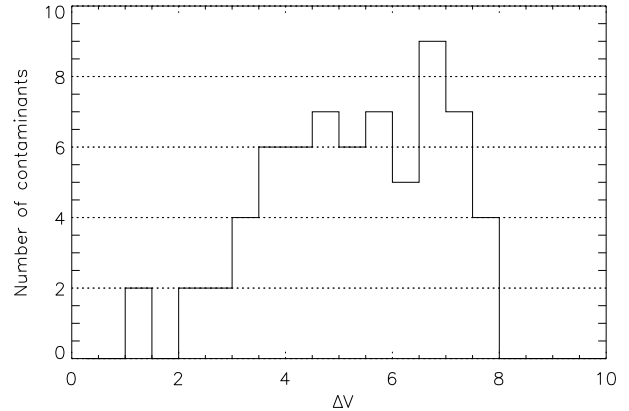
sensitivity to satellite jitter. Such defocusing increases the probability that the PSF of the star harbouring the planet overlaps the PSFs of nearby stars. None of the N2 coloured light curves is corrected for the fluxes of stars entering the target star mask. There is only an estimate of the contamination factors made with a generic mask before the run, but only for the white light curve. An analysis of the contamination effects in the *CoRoT* colours was performed in the case of CoRoT-8b only (Bordé et al. 2010). Since the quantitative evaluation of the contamination effect is necessary to compare transit depths in different colours, we applied a similar procedure by using the data available in the EXODAT database (Deleuil et al. 2009).

A preliminary step was the evaluation of the projected image on the CCD of the contaminant stars only, without the main target. We calculated the inflight PSF for each target and then we applied it to the nearest six contaminant stars (i.e., those listed in EXODAT), scaling the calculated PSF to match their *V* magnitudes and *B* – *V* colour indices. If the six EXODAT contaminants were all closer than 20 arcsec to the target, we completed the list with stars taken from the USNO-A2 catalogue, in order to be sure to include all the potential contaminating sources. Fig. 1 shows the histogram of the magnitude differences ΔV between the 67 contaminants and the stars harbouring planets. In two cases only we have $\Delta V < 2.0$ mag, related to contaminants far away from the main targets, i.e. 17.2 and 18.7 arcsec. This is not surprising, since the masks are actually chosen to minimize the contamination effect. However, although very small, this effect cannot be neglected for our purposes.

The above procedure supplied us a clear starting point, i.e. it allowed us to evaluate how many pixels of the target mask were contaminated by the flux from other stars, on the basis of their position, magnitude and colour. To proceed in the photometric analysis, we had to take into account not only the different colours of the stars but also the impossibility of having accurate photometric transformations between the *V* and *B* – *V* values and the spectral response of the specific mask+star combination.

To tackle this severe, intrinsic problem of the *CoRoT* photometry, we divided the calculated PSF of each contaminant into two parts, one bluer and one redder. We scaled the bluer part as the *B* mag and the redder part as the *V* mag with respect to the main target.

Then, we integrated the flux of the contaminants in the main mask and in the three submasks, comparing it with the flux produced by the main target. To estimate the contamination factor and

**Figure 1.** Histogram representing the *V* magnitude differences between the main targets and the contaminant stars. Bins refer to intervals of 0.5 mag.

its error bar we repeated the computations by running the procedure 20 000 times for each star. We left the parameters vary in wide ranges: the *B* and *V* magnitudes by ± 0.3 mag (and hence the *B* – *V* colour by ± 0.6 mag) and the center of the image of each star in a 3×3 pixel² box. The choice of these wide ranges was done for several reasons. EXODAT does not provide information about uncertainties on both magnitude and position of the contaminants, which are very faint stars. Moreover, the large error bar on the colour information is a way to take into account the impossibility of using the exact *CoRoT* spectral response on contaminants. The magnitude range also accounts for possible light variability. At the end of the process we chose the median values as the best estimate of the contamination factors and their error as the 68 per cent confidence interval (Table 1). The contamination factors for CoRoT-8b are in excellent agreement with those estimated by Bordé et al. (2010), i.e. 0.9, 0.7, 0.2, and 2.4 per cent for the white, red, green and blue *CoRoT* colours (hereafter W_C , R_C , G_C , B_C), respectively. This agreement strengthened our confidence in the adopted procedure.

The green submask is always composed of only one column of pixels: it acts as a separator between the blue and red spectra. As a consequence, the green flux is low compared to the others, and suffers from a higher dispersion. Hence we decided to disregard the G_C light curve, concentrating only on the R_C and B_C channels.

Table 2. List of the *CoRoT* planets analysed, with relative periods, ephemerides and masses taken from the discovery papers listed in Table 1.

Planet	Period (d)	$t_0 - 2450000$	Mass (M_J)
CoRoT-1b	1.5089557 ± 0.0000064	4159.4532	1.03
CoRoT-2b	1.74299641 ± 0.0000017	4706.4041	3.31
CoRoT-4b	9.20205 ± 0.00037	4141.36416	0.72
CoRoT-5b	4.0378962 ± 0.0000019	4400.19885	0.467
CoRoT-6b	8.886593 ± 0.000004	4702.2556	2.96
CoRoT-7b	0.853585 ± 0.000024	4398.0767	0.015
CoRoT-8b	6.21229 ± 0.00003	4238.9743	0.22
CoRoT-9b	95.2738 ± 0.0014	4603.3447	0.84
CoRoT-11b	2.99433 ± 0.000011	4597.679	2.33
CoRoT-3b	4.25695 ± 0.000005	4283.1383	21.66

2.2 Cleaning and detrending light curves

After having corrected each light curve with the contamination factor estimates, we analysed all the light curves separately, because trends and outliers are different in each colour.

We did not consider observations acquired when the satellite crossed the South Atlantic Anomaly and those flagged as inaccurate by the pipeline. After that, we analysed the *CoRoT* time series to study each planetary transit. The light curves are not linear: they show trends due to the ageing of detectors (Auvergne et al. 2009) and jumps due to hot pixels hit by cosmic rays. After the removal of obvious outliers, we calculated the average flux difference between two consecutive points. We deleted the points which were more than three times this quantity both from the previous and the next points.

Several algorithms have been proposed to detrend *CoRoT* light curves (e.g. Mazeh et al. 2009). We applied a specific approach for our purpose, i.e. having well-cleaned curves around the observed transits. We selected two intervals in the out-of-transit part of the light curves, before and after the central time of each transit T_i , where the light curve is expected to be flat, but actually is affected by stellar activity and instrumental trends (Fig. 2, top panel). As a rule, we considered the intervals $[T_i - 2.0 D, T_i - 0.7 D]$ and $[T_i + 0.7 D, T_i + 2.0 D]$, where D is the full duration of the transit. The data in these two intervals were fitted by a second-order polynomial. Then, we considered all the data in the interval $[T_i - 2.0 D, T_i + 2.0 D]$, and we divided them by the second-order fit, thus removing the trend and normalizing the flux units to the out-of-transit level (Fig. 2, bottom panel). In such a way, we also corrected for stellar activity. The calculated errors on all the detrending parameters have been propagated through the entire analysis; the errors on the orbital periods cited in the literature have also been taken into account when phase-folding the transits. We then superposed all the transits of each light curve using the periods determined in the discovery papers (Table 2) to obtain the phase-folded transits in each colour.

2.3 Limb darkening and transit fitting

The treatment of limb darkening in the fitting of planetary transits has long been analysed. Strong efforts were made to calculate the theoretical limb-darkening parameters, depending on the characteristics of the parent star and on the bandpass of the measurements (e.g. Claret 1998). With the coming of the *CoRoT* and *Kepler* space-based observatories, new effort was necessary to calculate new parameters for their ranges of sensitivity (Sing 2010;

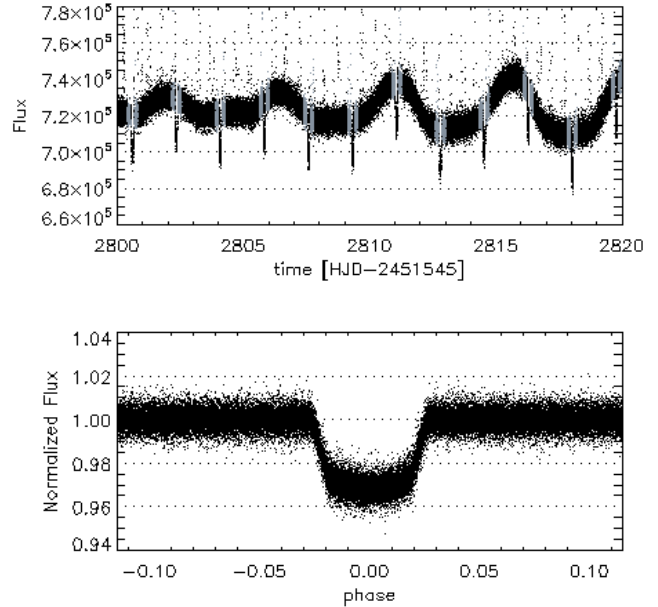


Figure 2. Example of how our algorithm works. Top: raw white light curve of CoRoT-2b, in grey are evidenced the data points we considered for the second order fit before and after each transit. Bottom: the final phase-folded transit of CoRoT-2b after the correction algorithm.

Claret & Bloemen 2011). However, no estimation has ever been made for the *CoRoT* colours. The *CoRoT* colours in fact are not bandpasses, because they are split by a low-dispersion device, and so the exact range of wavelengths slightly varies for each star, depending on its colour and position on the CCD; this lack of a precise photometric system is preventing the theoretical estimation of the limb-darkening coefficients. Howarth (2011) stresses how difficult it is to use standard and/or theoretical limb-darkening parameters when studying exoplanetary systems. We then decided to assume the general quadratic law for the limb-darkening effect only and to compute the μ_1 and μ_2 coefficients as free parameters in each case.

The phase-folded coloured light curves were fitted with the `TAP` package (Gazak et al. 2011), which uses the Mandel & Agol (2002) model for the transit shape. We performed a Markov Chain Monte Carlo analysis of 1000 000 steps for each planet, fitting simultaneously the 3 light curves (W_C , R_C , B_C) keeping the orbital period fixed. The inclination angle i , the distance between the planet and the star a (in units of the stellar radius R_s) and the transit timing t_0 were calculated considering all the colours simultaneously. On the other hand, the planet-to-star radius ratios R_p/R_s (the square root of the transit depth) and the limb-darkening coefficients μ_1 and μ_2 were calculated for each colour (Table 3). The limb-darkening parameters tabulated by Sing (2010) for the *CoRoT* range of sensitivity are within the error bars of our values for the W_C light curves (Table 4), thus corroborating our methodological approach. The reported error bars are calculated by propagating the errors on the parameters (the long-term trend in different colours, the orbital periods and the contamination effects) we used to extract the shape of the transit from the light curves.

Regarding the orbital parameters, all orbits were considered to be circular, except for CoRoT-5b ($e = 0.07 \pm 0.06$) and CoRoT-9b ($e = 0.07 \pm 0.05$), for which eccentricities were left as free parameters but constrained around the values found in literature. The resulting

Table 3. Fit results for the phase-folded transits of the planets analysed, with planet-to-star radius ratios and limb-darkening coefficients (linear and quadratic) for the R_C and B_C colours. The orbital periods are taken from the discovery papers.

Planet	a/R_s	i ($^\circ$)	R_p/R_s		μ_1		μ_2	
			R_C	B_C	R_C	B_C	R_C	B_C
CoRoT-1b	4.72 ± 0.17	83.8 ± 1.0	0.1440 ± 0.0028	0.1471 ± 0.0030	0.58 ± 0.31	0.34 ± 0.27	-0.16 ± 0.45	0.38 ± 0.38
CoRoT-2b	6.76 ± 0.09	88.06 ± 0.72	0.1655 ± 0.0015	0.1665 ± 0.0021	0.38 ± 0.10	0.55 ± 0.20	0.03 ± 0.21	0.06 ± 0.33
CoRoT-4b	16.60 ± 1.05	89.01 ± 0.75	0.1067 ± 0.0025	0.1052 ± 0.0041	0.40 ± 0.29	0.55 ± 0.31	-0.01 ± 0.41	-0.03 ± 0.44
CoRoT-5b	9.44 ± 0.77	85.55 ± 0.72	0.1144 ± 0.0030	0.1104 ± 0.0050	0.45 ± 0.30	0.54 ± 0.35	0.00 ± 0.39	0.08 ± 0.47
CoRoT-6b	17.96 ± 0.89	89.04 ± 0.61	0.1152 ± 0.0024	0.1174 ± 0.0031	0.29 ± 0.23	0.51 ± 0.29	0.20 ± 0.41	0.00 ± 0.45
CoRoT-7b	5.40 ± 1.10	84.8 ± 4.5	0.0182 ± 0.0015	0.0158 ± 0.0088	0.63 ± 0.29	0.45 ± 0.35	0.01 ± 0.39	0.00 ± 0.38
CoRoT-8b	18.3 ± 2.7	88.56 ± 1.03	0.0811 ± 0.0034	0.0755 ± 0.0072	0.58 ± 0.30	0.50 ± 0.32	-0.07 ± 0.41	0.04 ± 0.39
CoRoT-9b	96.5 ± 5.0	89.84 ± 0.12	0.1144 ± 0.0026	0.1202 ± 0.0042	0.42 ± 0.32	0.42 ± 0.34	-0.11 ± 0.48	0.07 ± 0.44
CoRoT-11b	6.71 ± 0.37	82.86 ± 0.62	0.1009 ± 0.0034	0.1031 ± 0.0024	0.44 ± 0.34	0.52 ± 0.33	0.05 ± 0.41	-0.04 ± 0.38
CoRoT-3b	8.3 ± 1.3	86.5 ± 2.6	0.0686 ± 0.0030	0.0603 ± 0.0080	0.52 ± 0.35	0.52 ± 0.34	-0.15 ± 0.49	0.00 ± 0.39

Table 4. Comparison between fitted limb-darkening coefficients on the W_C light curves and those estimated by Sing (2010) for the *CoRoT* range of sensitivity.

Planet	μ_1		μ_2	
	W_C	Sing	W_C	Sing
CoRoT-1b	0.51 ± 0.27	0.37	-0.03 ± 0.40	0.27
CoRoT-2b	0.43 ± 0.10	0.46	0.02 ± 0.20	0.22
CoRoT-4b	0.43 ± 0.36	0.37	0.04 ± 0.52	0.28
CoRoT-5b	0.37 ± 0.31	0.37	0.11 ± 0.38	0.27
CoRoT-6b	0.36 ± 0.26	0.38	0.09 ± 0.43	0.27
CoRoT-7b	0.48 ± 0.35	0.53	-0.02 ± 0.49	0.17
CoRoT-8b	0.52 ± 0.31	0.59	-0.03 ± 0.40	0.12
CoRoT-9b	0.54 ± 0.25	0.46	0.17 ± 0.37	0.22
CoRoT-11b	0.46 ± 0.34	0.34	0.02 ± 0.40	0.29
CoRoT-3b	0.44 ± 0.34	0.32	0.00 ± 0.43	0.31

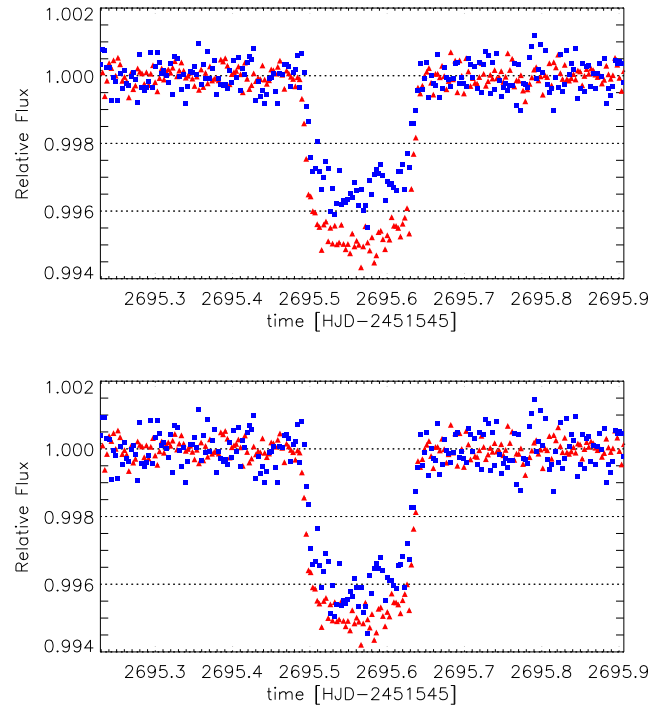
values of the inclination angle and of a/R_s are all within the error bars of those given in the discovery papers.

We also investigated the possibility that the decision to fit simultaneously the limb-darkening parameters could have affected the R_p/R_s determinations. We repeated the same fitting procedure keeping fixed the linear μ_1 parameters to the median values (0.44 for R_C , 0.51 for B_C). We obtained the same values for the radius ratios, with negligible differences with respect to the values listed in Table 3.

2.4 The case of CoRoT-3b

With its mass of $21.66 M_J$ (Deleuil et al. 2008), CoRoT-3b was defined as an inhabitant of the ‘brown dwarf desert’. It could be a low-mass brown dwarf or the member of a new class of ‘superplanets’, because it is on the edge between planets and stars. Therefore, we did not consider it as a bona-fide member of our class of exoplanets, but the presence of two close stars 2.9 and 4.9 mag fainter at distances of 5.6 and 5.3 arcsec, respectively (Deleuil et al. 2008), makes its analysis very challenging for the relevance of the contamination (Table 1).

The light curves of the original chromatic data, without applying any correction for the contaminant stars, show a clear difference of 0.002 in relative flux in the depths of the transits (Fig. 3, upper panel). After applying our method to remove the contamination using the photometry listed in EXODAT, this amount is halved

**Figure 3.** Transits of CoRoT-3b in the R_C (triangles) and B_C (squares) colours, before (*top*) and after (*bottom*) removing the contamination of nearby stars. Points refer to a binning of 0.003 d.

(Fig. 3, lower panel), confirming that our procedure works in the right direction. The resulting difference between the radii in R_C and B_C is still large (~ 12 per cent, see Table 3), but the scattered B_C light curve and its quite large error bar makes the values of the radii compatible in this extremely contaminated case. In Fig. 3 a small ‘bump’ is also notable at the bottom of the B_C transit. Due to the fact that the orbital period of CoRoT-3b is compatible with a synchronization with the stellar rotation (Mazeh & Faigler 2010), we cannot exclude it to be an inhomogeneity on the surface of the F3V parent star. We also should not forget the specificity of the nature of the CoRoT-3 system. For the sake of completeness, we calculated that a missed bright contaminating star with $V=16.0$ and $B-V=+0.3$ could equalize the depths of the transits when affecting

the B_C contamination up to 35 per cent. Undetected or undetectable contaminant stars, especially in the crowded field of the Galactic plane observed by *CoRoT*, constitute a possible error source we cannot quantify. However, at the moment, there is no evidence of a missed contaminating star around CoRoT-3 (Deleuil et al. 2008).

3 DISCUSSION

The planet-to-star radius ratios in the R_C and B_C colours (Table 3) provide the expected evidence that the transits are mostly achromatic. In several cases, the ratio values are far from equality, but the error bars recover it in all cases except for CoRoT-9b. Therefore, we looked at the whole set of planet-to-star radius ratios to verify if the ensemble analysis could provide some hints of departures from equality. To do that we used the distance from the parent star, the mass of the planet and the effective temperature of the planet. We obtained the plot shown in Fig. 4 when sorting the planet-to-star radius ratios in function of the planet’s mass. We can see that all the planets with a B_C radius smaller than the R_C radius are confined in the $M < 0.8 M_J$ region. We checked if such behaviour could depend from the contamination level, but the plot did not change by varying the contamination factors up to 30 per cent of the value calculated by using the procedure described in Section 2.1. This could mean that the R_C radius of the low-mass planets is larger than the B_C radius, while for massive planets the radii are almost equal (Fig. 5). The statistics is very limited at the moment and the fact that all the planets with $M < 0.8 M_J$ are below the equality line could be fortuitous, also considering that they are those with the bigger error bars. For the sake of completeness, we verified if the behaviour sketched by Figs. 4 and 5 can reflect some physical reason. Tessenyi et al. (2012) stated that the height of a planet’s atmosphere can be estimated to be $\Delta z = nH$, where typically $n \sim 5$ and H is the atmospheric scaleheight. Since $H = \frac{kT}{\mu g}$ ¹, the smaller gravity of low-mass planets results in a larger atmospheric scaleheight, and this could enhance the atmospheric features in the photometric measurements at different wavelengths. We also verified that the observed transit depth differences of some hundreds of ppm are consistent with the effects of planetary atmospheres. In the specific case of the *CoRoT* planets, we obtained values of Δz in the range 0.5-5 per cent of the radius of the planet (even more for CoRoT-7b). These values of the atmospheric height correspond to upper limits on transit depth differences due to an atmospheric absorption of 100-1300 ppm.

We searched for other transiting planets with transit depth measurements in multiple optical bandpasses. The characterization of the planetary atmosphere of HD 189733b ($M = 1.138 M_J$) supplied evidences of the presence of high-altitude atmospheric haze detected in the visible (Pont et al. 2008; Lecavelier Des Etangs et al. 2008; Sing et al. 2011) and probably extended to the infrared (Gibson et al. 2012). The transmission spectrum is in good agreement with that of Rayleigh scattering and the planetary radius results to be slightly smaller at long wavelengths, in agreement with the results obtained from *CoRoT* photometry (Fig. 5). The mass of HD 209458b ($M = 0.69 M_J$) is too close to the value $0.8 M_J$ to provide a useful check on the dependence of the planet-to-star radius ratios on the mass, but we note that Knutson et al. (2007) obtained different radius values in function of wavelength in the

¹ k is the Boltzmann constant, T the equilibrium temperature of the planet, μ the mean molecular mass of the atmosphere and g the gravity acceleration.

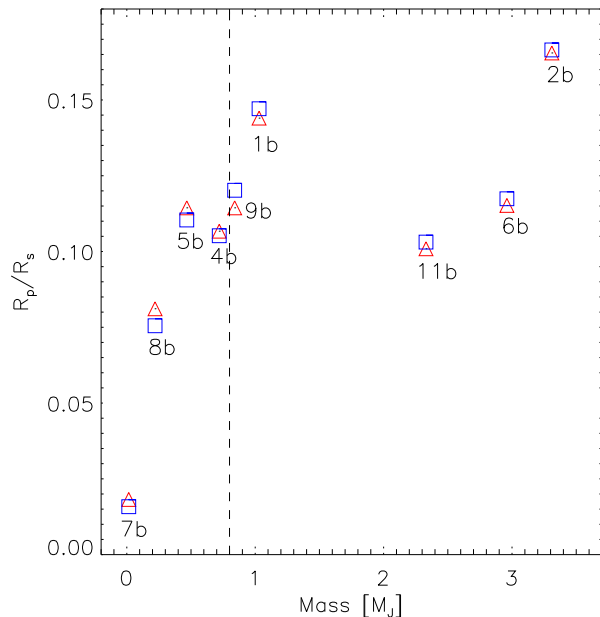


Figure 4. Planet-to-star radius ratios of the *CoRoT* planets analysed in the R_C (triangles) and B_C (squares) colours. Error bars are of the order of the point dimension (except for CoRoT-7b which are about twice the point dimension).

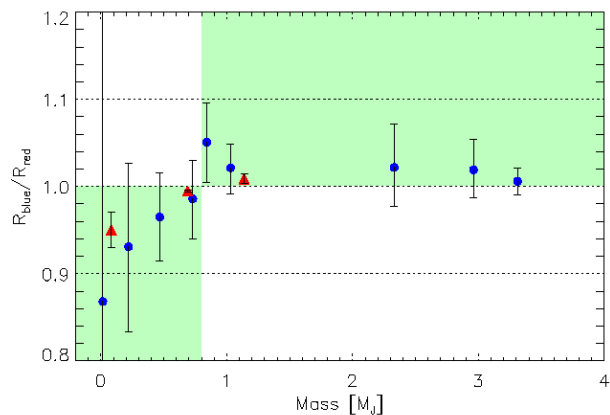


Figure 5. Radius of the planet in the B_C colour with respect to the radius in the R_C colour. Blue circles refer to our analysis of *CoRoT* planets. The huge error bars of CoRoT-7b, not even completely inside the plot, are due to the very small depths of the transit with respect to the S/N, especially in the B_C colour. Red triangles refer to literature data (cited in Section 3) taken in different optical bandpasses: R_{blue} refers to the measurement with the shorter wavelength, and R_{red} to the measurement with the longer one.

full range from 293 to 1019 nm. Theoretical transmission spectra support such transit depth variations (Gillon et al. 2012, see their fig. 7). With a mass of only $0.081 M_J$, HAT-P-11b could provide a significant test. Deming et al. (2011) pointed out that the radius ratio is 6 per cent larger in the J band than in the *Kepler* photometry. They are not able to provide an explanation for such a large discrepancy and suggest a variable contribution of the water absorption in the Earth’s atmosphere during the observations.

4 CONCLUSIONS

We provided a methodological approach to extract the chromatic information contained in the light curves of 10 transiting planets discovered by *CoRoT*. We satisfactorily removed the contaminating light coming from poorly known stars inside the pre-defined aperture masks. This step is of extreme importance for a coherent analysis of transits, as third light can affect in different percentages the chromatic light curves and thus bring to incongruous comparisons between the different colours. When comparing transits of the same planet observed with different instruments (or at different wavelengths), an analysis of the contamination effect is fundamental, since third light could lead to different and erroneous transit depth (and planetary radius) estimations.

Then we detrended and cleaned the data producing a homogeneous set of light curves in each of the *CoRoT* colours. The analysis of the *CoRoT* chromatic light curves confirms that all the transit depths for the planets studied in two different colours are nearly equal. However, we could put in evidence an interesting behaviour of the planet-to-star radius ratios of the transits in B_C and R_C colours when they are plotted versus the mass of the planets. We suggest the possibility of observing departures from transit depth equality for planets having $M < 0.8 M_J$. This hypothesis is still rather speculative at the moment, but is not groundless, roughly reflecting the relevance of the atmospheric scale height in low-mass planets. The inclusion of the Na D lines in the range of the R_C colour (Léger et al. 2009) could also play a role when considering that Sing et al. (2008a, 2008b) report on the very strong absorption of the Na D lines in the high atmosphere of HD 209458b, around 589 nm. Of course, the results would have been more compelling if the *CoRoT* photometric system was a standard or a well-calibrated one.

The careful evaluation of the chromatic effect could result in a fertile exercise in the case of low-mass planets. High-precision multicolour photometry of transits could provide an efficient tool to investigate the upper atmosphere of exoplanets, taking into account the intrinsic difficulties inherent in accessing these thin layers in other worlds' atmospheres.

ACKNOWLEDGMENTS

The authors wish to thank D. Pollacco for useful comments on a first draft of the manuscript, J. Vialle for checking the English form, and the anonymous referee for the suggestions aimed at improving the presentation of the results. FB acknowledges financial support from the ASI-Università di Padova Contract I/044/10/0. EP acknowledges financial support from the PRIN-INAF 2010 *Asteroseismology: looking inside the stars*.

References

- Aigrain, S., Collier Cameron, A., Ollivier, M., et al. 2008, *A&A*, 488, L43
- Alonso, R., Auvergne, M., Baglin, A., et al. 2008, *A&A*, 482, L21
- Auvergne, M., Bodin, P., Boisnard, L., et al. 2009, *A&A*, 506, 411
- Baglin, A., Auvergne, M., Barge, P., et al. 2006, *ESA Special Publication*, 1306, 33
- Barge, P., Baglin, A., Auvergne, M., et al. 2008, *A&A*, 482, L17
- Barge, P., Léger, A., Ollivier, M., et al. 2006, *ESA Special Publication*, 1306, 83
- Bordé, P., Bouchy, F., Deleuil, M., et al. 2010, *A&A*, 520, A66
- Borucki, W. J., Koch, D. G., Basri, G., et al. 2011, *ApJ*, 736, 19
- Carpano, S., Cabrera, J., Alonso, R., et al. 2009, *A&A*, 506, 491
- Claret, A. 1998, *VizieR Online Data Catalog*, 3335, 50647
- Claret, A., & Bloemen, S. 2011, *A&A*, 529, A75
- Deeg, H. J., Moutou, C., Erikson, A., et al. 2010, *Nature*, 464, 384
- Deleuil, M., Deeg, H. J., Alonso, R., et al. 2008, *A&A*, 491, 889
- Deleuil, M., Meunier, J. C., Moutou, C., et al. 2009, *AJ*, 138, 649
- Deming, D., Sada, P. V., Jackson, B., et al. 2011, *ApJ*, 740, 33
- Fridlund, M., Hébrard, G., Alonso, R., et al. 2010, *A&A*, 512, A14
- Gandolfi, D., Hébrard, G., Alonso, R., et al. 2010, *A&A*, 524, A55
- Gazak, J. Z., Johnson, J. A., Tonry, J., et al. 2011, *Astrophysics Source Code Library*, 6014
- Gibson, N. P., Aigrain, S., Pont, F., et al. 2012, *MNRAS*, 422, 753
- Gillon, M., Demory, B.-O., Benneke, B., et al. 2012, *A&A*, 539, A28
- Howarth, I. D. 2011, *MNRAS*, 418, 1165
- Knutson, H. A., Charbonneau, D., Noyes, R. W., et al. 2007, *ApJ*, 655, 564
- Lecavelier Des Etangs, A., Pont, F., Vidal-Madjar, A., & Sing, D. 2008, *A&A*, 481, L83
- Léger, A., Rouan, D., Schneider, J., et al. 2009, *A&A*, 506, 287
- Mandel, K., & Agol, E. 2002, *ApJ*, 580, L171
- Mayor, M., Marmier, M., Lovis, C., et al. 2011, arXiv:1109.2497
- Mazeh, T., & Faigler, S. 2010, *A&A*, 521, L59
- Mazeh, T., Guterman, P., Aigrain, S., et al. 2009, *A&A*, 506, 431
- Pont, F., Knutson, H., Gilliland, R. L., et al. 2008, *MNRAS*, 385, 109
- Poretti, E., Rainer, M., Weiss, W. W., et al. 2011, *A&A*, 528, A147
- Rauer, H., Queloz, D., Csizmadia, S., et al. 2009, *A&A*, 506, 281
- Seager, S., & Deming, D. 2010, *ARA&A*, 48, 631
- Sing, D. K. 2010, *A&A*, 510, A21
- Sing, D. K., Pont, F., Aigrain, S., et al. 2011, *MNRAS*, 416, 1443
- Sing, D. K., Vidal-Madjar, A., Désert, J.-M., et al. 2008, *ApJ*, 686, 658
- Sing, D. K., Vidal-Madjar, A., Lecavelier des Etangs, A., et al. 2008, *ApJ*, 686, 667
- Tessenyi, M., Ollivier, M., Tinetti, G., et al. 2012, *ApJ*, 746, 45